Crystallization and Orientation of Syndiotactic Polystyrene in Nanorods

Hui Wu, Wei Wang, Huixian Yang, and Zhaohui Su*

State Key Laboratory of Polymer Physics and Chemistry, Changchun Institute of Applied Chemistry, Chinese Academy of Sciences, and Graduate School of Chinese Academy of Sciences, Changchun, Jilin 130022, P. R. China

Received March 8, 2007; Revised Manuscript Received April 5, 2007

ABSTRACT: Syndiotactic polystyrene (sPS) nanorods of 200 and 80 nm diameters were prepared by infiltrating porous anodic alumina oxide templates with polymer melt, and the crystallinity and orientation of various forms of sPS crystals in the nanorods were studied by FTIR spectroscopy and electron diffraction. For sPS crystallized from amorphous state at lower temperatures, α-form crystals were found in the nanorods with random orientation and the same degree of crystallinity as that in the bulk. However, for sPS crystallized from molten state at 260 °C, while no preferred orientation was found for the chains in the melt, the β-crystals formed in the nanorods oriented preferentially with the *c*-axis aligning perpendicular to the axial direction of the nanorod, and the degree of crystallinity was significantly lower than that in the bulk. The crystallinity decrease was more profound for nanorods of smaller diameter. These results were also supported by electron diffraction data and can be attributed to competition between nucleation and crystal growth in the nanotemplates.

Introduction

Polymer nanotubes and nanorods are of scientific and technological interest because they have potential applications in many areas, such as microelectronics, optical, mechanical, and biomedical devices.[1,2] Among the various preparation methods developed for polymer nanotubes and nanorods, template-based approaches have been the subject of intensive research.[1−10] Martin et al. have explored a general method termed *template synthesis* for preparation of tubular and fibrillar micro- and nanostructures, which entails synthesizing the desired material within the pores of a nanoporous template membrane.[1−3] Another type of versatile and simple approach involves wetting of porous templates by polymer melts or solutions for the fabrication of polymer nanotubes and nanorods.[4,5] Vacuum filtration of a polymer solution through a nanoporous template membrane can also yield polymer nanotubes.[6] The anodic aluminum oxide (AAO) membranes possessing straight, rigid, separated, and monodisperse cylindrical pores are ideal templates for these methods for the preparation of nanotubes and nanorods with monodisperse diameters in the nanometer to micrometer scales.[5]

For nanomaterials their internal morphology largely determines their mechanical, optical, and electrical properties. At the same time they are good subjects for both experimental and theoretical studies on behavior and properties of polymers under confinement. It has been well-established that phase-separating block copolymers can be frustrated and exhibit new morphologies due to the confinement and the curvature effects when forced into cylindrical pores.[11−15] For example, nanorods of styrene/butadiene diblock copolymers prepared by capillary action in AAO templates have been studied, and new morphologies observed not accessible by other means due to the confinement imposed by the curvature of the nanopore and the diameter incommensurate with the scale of the phase-separated microdomains.[11−14] The diameter dependence of the morphology was also studied for a symmetrical polystyrene-*block*-poly(methyl methacrylate) copolymer confined within pores of AAO templates with the diameter varying from 25 to 400 nm.[15] The materials used in these studies were amorphous, and the experimental technique employed was transmission electron microscopy (TEM).

In addition to block copolymers, studies on the morphologies of homopolymers in nanotubes and nanofibrils have been reported.[16−22] It was found that conductive polymers synthesized in nanotemplates can exhibit orientation parallel[16,17] or perpendicular[18−20] to the axis of the tubules and fibrils. For semicrystalline materials, the degree of crystallinity and the orientation of the crystalline domains are important factors in controlling the physical properties of the material. It has been reported[21,22] that the crystallites of poly(vinylidene difluoride) (PVDF) grow preferentially in the tube direction when the nanotubes are prepared by wetting the template with PVDF melts, while the PVDF nanotubes prepared from solution are amorphous; the orientation of the PVDF chains prior to crystallization was speculated to be responsible for the difference in the crystallinity observed.[21] It was also concluded that the crystal orientation is controlled by the kinetics of nucleation and growth under 2D confinement.[22] In another study, it was found that PVDF crystallized in the nanotrenches orients with the chain axis parallel to the walls.[23] In addition, studies on poly(ethylene oxide) (PEO) crystallization confined in nanocylinders resulting from phase separation in block copolymer films indicate that the orientation of the PEO crystals is dependent on the crystallization temperature.[24,25] However, no comparison was made between the degrees of crystallinity for the polymer in the nanostructures and in the bulk (film) in these reports.

Syndiotactic polystyrene (sPS) is a semicrystalline polymer with good thermal and chemical stability and has received considerable attention recently.[26,27] The polymer exhibits rapid crystallization rate, high crystallinity, and high melting temperature (ca. 270 °C) due to the high stereoregularity of the polymer chains.[28] Furthermore, the polymer exhibits complicated polymorphic structures (involving four stable crystalline

* To whom all correspondence should be addressed: Tel (86)431-85262854; Fax (86)431-85262126; e-mail zhsu@ciac.jl.cn.

10.1021/ma070564o CCC: $37.00
Published on Web 05/16/2007

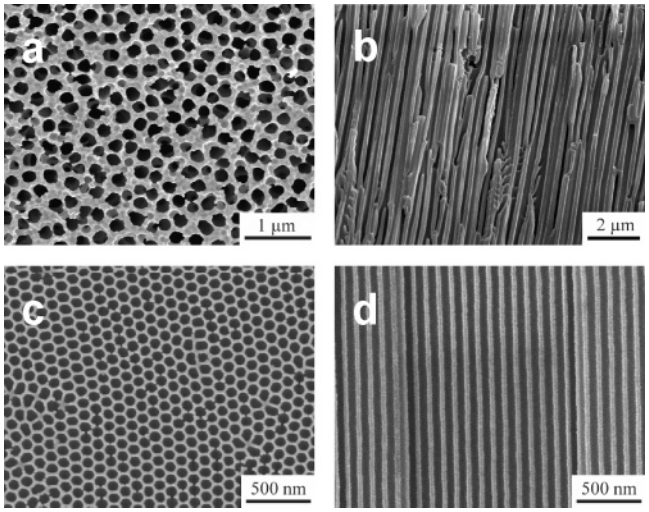

Figure 1. FE-SEM micrographs of AAO templates: (a, b) 200 nm (Whatman); (c, d) 80 nm. (a, c) Top view of the AAO templates; (b, d) cross section of the AAO templates.

forms: α, *β*, *γ*, and *δ*) and solid−solid phase transition behavior.[28−35] It has been shown that the *γ*- and *δ*-forms, both containing s(2/1)2 helical chains, can be formed under solvent treatment, while the α- and *β*-forms, both containing planar zigzag chains, can be obtained from melt or glassy state under different thermal conditions. The crystal structure of the *β*-form is characterized by the orthorhombic unit cell with parameters of $a = 8.81$ Å, $b = 28.82$ Å, and $c = 5.04$ Å,[31,32] and that of the α-form consists of hexagonal unit cells with parameters of $a = b = 26.26$ Å and $c = 5.04$ Å.[33] The characteristic vibrational bands associated with various sPS microstructures and morphologies have been well established,[35,36] making it convenient to investigate sPS nanorods using the vibrational spectroscopy technique.

In the present study, we prepared various diameter sPS nanorods with different crystalline forms by infiltrating polymer melts into AAO templates and investigated the morphology of the polymer in the nanorods and in the bulk using Fourier transform infrared (FTIR) spectroscopy, which is capable of assessing conformations and orientation of polymer chains not only in the crystalline domains but also in the amorphous state. The degree of crystallinity was determined, and the orientations of both the crystalline domains and the amorphous chains were analyzed. Our results are reported here.

Experimental Section

Anodic Aluminum Oxide (AAO) Templates. The ordered AAO templates with 200 nm pore diameter and 60 *μ*m pore depth were purchased from Whatman, while AAO templates with 80 nm pore diameter and 75 *μ*m pore depth were prepared via a two-step anodization process. Details on the anodization process are described in the literature.[37,38] Figure 1 shows the SEM micrographs of the AAO templates. The templates are comprised of straight, cylindrical pores, orienting normal to the disk surface. Prior to use, they were ultrasonicated in solvents of different polarity, such as deionized water, ethanol, acetone, chloroform, and hexane.

Preparation of sPS Nanorods. Syndiotactic polystyrene (sPS) pellets (Dow Questra F-2250, $M_w \sim 260\,000$) were obtained from Dow Chemical Co. and used as received. Transparent amorphous sPS film with a thickness of ∼120 *μ*m was obtained by compression-molding several sPS pellets at 300 °C for 4 min and quickly quenching the film in ice water. The alumina membrane was placed on top of the sPS film supported by a glass slide, and the assembly was heated at 300 °C for 20 min under a nitrogen atmosphere so that the sPS melt was drawn into the membrane pores by capillary force. Thermal gravimetric analysis indicates no detectable degradation under this condition (data not shown). The experimental temperatures were chosen according to the literature[39] to obtain different crystalline forms. The assembly was cooled from the molten state to 260 °C in 20 min and maintained for 2 h to anneal the sPS and then cooled to room temperature to yield *β*-form sPS, while the amorphous sample was produced by quickly quenching the template/polymer assembly in ice water. The α-form sPS was prepared by heating the amorphous sample assembly from room temperature to 240 °C and annealing at this temperature for 2 h. The template/polymer assembly was then immersed in a sodium hydroxide aqueous solution (1.0 mol/L) for 12 h to remove the AAO template, leaving an array of sPS nanorods protruding from the sPS film. Four crystalline films for each sample were prepared separately for FTIR analyses.

Electron Microscopy. The morphology of the sPS nanorods was investigated using an FEL XL30 ESEM field emission scanning electron microscope. Before the FESEM observation, a thin layer of Au was coated on the sample surface. Bright field transmission electron microscopy (TEM) and electron diffraction (ED) were performed on a JEOL 1011 TEM operating at an accelerating voltage of 100 kV. To obtain a single nanorod specimen, an sPS film with protruding nanorods was ultrasonicated in methanol for 30 min, and a drop of the methanol with the suspending nanorods was allowed to dry on a carbon-coated copper grid. The ED spacing was calibrated against the diffraction of gold, and the rotation between the bright field images and the diffraction pattern was calibrated by measuring the angle between the [001] diffraction and the long edge of a molybdenum trioxide crystal which is known to be [001].

Infrared Spectroscopy. Thin slices of the cross section of an sPS film with protruding nanorods were cut under an optical microscope using a razor blade. Infrared measurements were performed on a Bruker IFS 66V/S FTIR spectrometer in connection with a Bruker Hyperion 3000 IR microscope equipped with a narrow band mercury−cadmium telluride (MCT) detector operating in the transmission mode. The spectra were collected at 2 cm^{-1} resolution with 256 scans coadded. Curve fitting was performed using the Levenberg−Maquardt least-squares algorithm routine of the OPUS software package, and the residual rms error was about 0.002. Polarized spectra were collected with a gold wire grid polarizer (Specac) mounted between the sample and the detector optics. The growth direction of the nanorods was defined as the reference direction, and the infrared beam passing through the sample at normal incidence was polarized parallel or perpendicular to the reference direction accordingly (Figure 3). Generally 512 scans were collected at 2 cm^{-1} resolution for each polarized IR spectrum. The orientation function F can be determined from the infrared dichroism[40] through

$$F = \frac{3\langle\cos^2\theta\rangle - 1}{2} = \frac{R-1}{R+2}\frac{R_0+2}{R_0-1} \qquad (1)$$

where θ is the angle between the chain axis and the nanorod axis (reference axis), R is the infrared dichroic ratio defined as $R = A_{\parallel}/A_{\perp}$, $A_{\parallel}$ and $A_{\perp}$ being the absorbances with the infrared beam polarized parallel and perpendicular to the direction of the long axis of the nanorods, respectively, and $R_0 = 2\cot^2\alpha$, where α is the angle between the chain axis and the transition moment associated with the infrared band used for the orientation measurements. For measuring uniaxial orientation, the orientation function F ranges from −0.5 to 1. A perfect parallel orientation leads to $F = 1$, while a perfect perpendicular orientation gives $F = -0.5$, and a random orientation is indicated by $F = 0$.

Results and Discussion

Generally, the viscosity of a crystalline polymer drops quickly when heated to above its melting point. Porous anodic aluminum oxide templates are known to have high-energy surface and can be wet easily by polymer melts.[5] The wetting of the pore walls

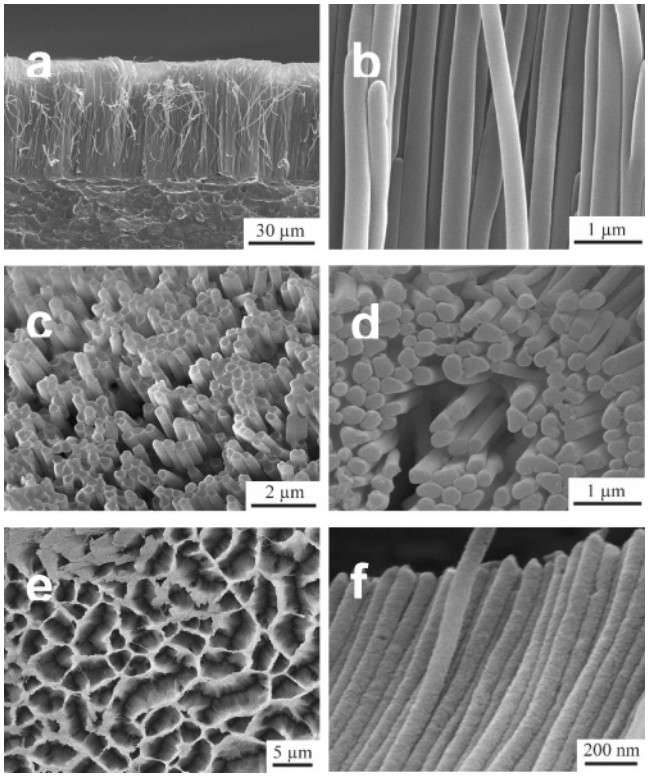

Figure 2. FE-SEM micrographs of sPS nanorods prepared by infiltrating AAO template with a sPS melt: (a, b, c, d) 200 nm; (e, f) 80 nm. (a, b, f) Cross section of the nanorod array; (c, e) top view of the nanorod array; (d) top view of the nanorod array with the tips of the nanorods removed.

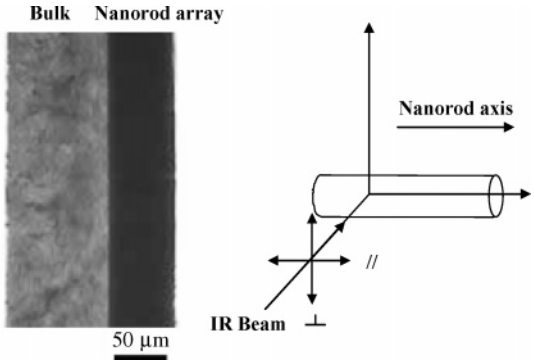

Figure 3. Optical micrograph of a thin slice of the sPS film with nanorods for infrared analysis with the reference coordinate depicted. The darker section is the nanorod array.

by the sPS melt causes a capillary rise of the polymer melt into the nanopores, leading to sPS nanorods. The SEM micrographs of the sPS nanostructure protruding from the substrate film with the AAO template removed are shown in Figure 2. The diameters of the nanorods are quite uniform, and meniscuses on the tips of the rods are clearly observed, indicating that the wetting of the AAO template by the sPS melt was driven by capillary force.[10] The nanorods all align well, with the rods generally growing in the direction normal to the film surface. This direction is defined as the reference direction in the FTIR study to be discussed later. The length of the nanorods was up to 60 μm, which was the thickness of the AAO templates. The thickness of the residual sPS film (bulk) beneath the nanorod array was ~90 μm. The dimensions are confirmed by the micrograph of a micro-FTIR specimen taken in the transmission mode (Figure 3). The area on the right is the nanorod array, which appears darker due to the scattering of light at the

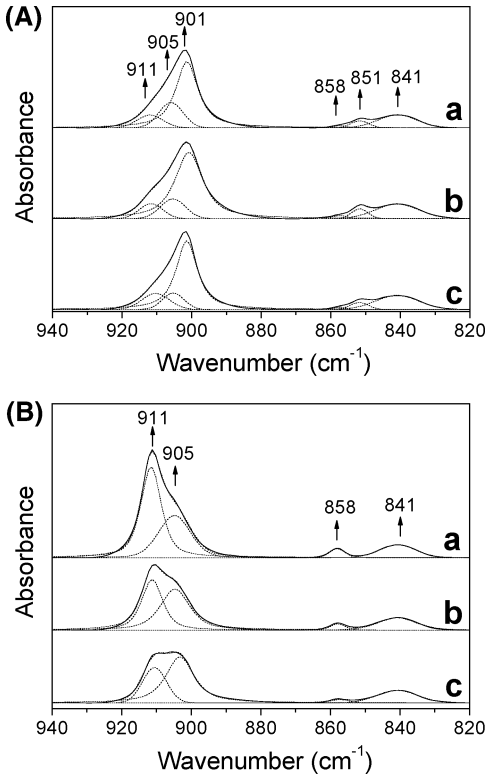

Figure 4. Infrared spectra of the sPS crystallized at lower temperatures (A) and at 260 °C (B). In both figures, (a) is the spectrum for the bulk, (b) is for the 200 nm nanorods, and (c) is for the 80 nm nanorods. The dash lines are the deconvoluted peaks, and the dotted lines are the fitted curves.

numerous nanorod/air interfaces, while the translucent section on the left is a cross section of the residual sPS film with a thickness of ~90 μm.

To assess the sPS crystallinity, the polymer in the bulk and in the nanorods was examined using FTIR spectroscopy. Since the nanorods and the bulk were connected (see Figures 1 and 2) and treated together, they experienced the same thermal history. The 940−820 cm^{-1} regions where the bands characteristic of different morphologies are present[41−43] of the FTIR spectra for the sPS nanorods and the bulk obtained under different conditions are shown in Figure 4.

For sPS crystallizes at lower temperature from amorphous state, the spectra for the bulk and the nanorods are almost the same (Figure 4A). The predominant features of all three spectra are the 901 and 851 cm^{-1} bands characteristic of the α-form structure and the amorphous bands at 905 and 841 cm^{-1}, and the characteristic bands of the β-phase at 911 and 858 cm^{-1} are small, indicating that the crystalline phase is mainly α when sPS is crystallized at lower temperature, in agreement with the literature.[39] The degree of crystallinity can also be analyzed quantitatively by FTIR using the bands in the 870−820 cm^{-1} region and the following equations:[41−43]

$$C_\beta = \frac{A_{858}/a_\beta}{A_{841} + A_{851}/a_\alpha + A_{858}/a_\beta} \times 100\%,$$

$$C_\alpha = \frac{A_{858}/a_\alpha}{A_{841} + A_{851}/a_\alpha + A_{858}/a_\beta} \times 100\% \quad (2)$$

where C_β represents the β form crystallinity, A_{841}, A_{851}, and A_{858} are the respective band areas for amorphous, α-form, and β-form crystals, and a_α and a_β are the absorptivity ratios for α- and β-form vs amorphous, which are 0.178 and 0.272, respec-

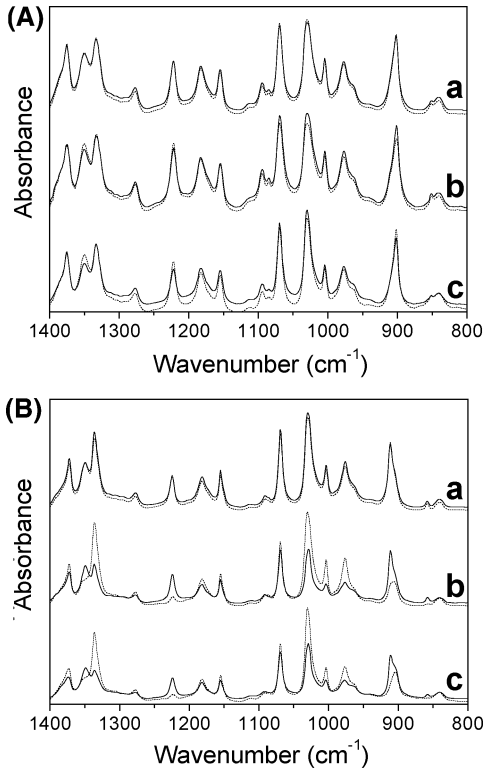

Figure 5. Polarized infrared spectra of the sPS crystallized at lower temperatures (A) and at 260 °C (B). (a) represents the bulk, (b) the 200 nm nanorods, and (c) the 80 nm nanorods: perpendicular polarization (—); parallel polarization (---).

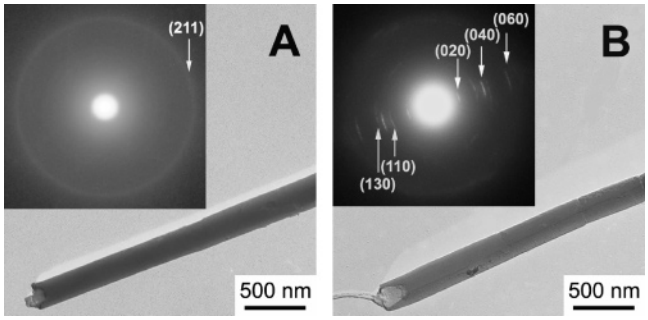

Figure 6. TEM images of a single sPS nanorod crystallized at lower temperatures (A) and at 260 °C (B). The inset is the corresponding electron diffraction pattern.

tively.[41−43] Using eq 2, the crystallinity of the α-form sPS in the nanorods of 80 and 200 nm diameters and the bulk was 57.4%, 58.6%, and 61.5%, and that of the *β*-form was 6.3%, 6.6%, and 6.7%, respectively. Therefore, for sPS crystallizing at lower temperature, we observed no significant difference in the degree of crystallinity between the nanorods and the bulk. For sPS crystallizing at higher temperature, however, the case is different. From Figure 4B it can be observed that for both the nanorods and the bulk, besides the amorphous bands at 905 and 841 cm^{-1}, the characteristic bands of the *β*-form crystalline phase at 911 and 858 cm^{-1} are present, while the 901 and 851 cm^{-1} bands associated with the α-form crystals are not observed. This indicates that sPS crystallizes into *β*-form at 260 °C, as reported in the literature[39] in both the bulk and the nanorods. This was also verified by electron diffraction (ED) pattern shown as the inset of Figure 6. By qualitatively comparing the three spectra, it is apparent that the relative intensities of the crystalline bands with respect to the amorphous bands for the nanorods are weaker than that for the bulk, revealing lower sPS crystallinity in the nanorods. Four replicate nanorod arrays were fabricated for each diameter and measured, and the average crystallinities thus obtained for the nanorods of 80 and 200 nm diameters and the bulk were 36.2%, 49.8%, and 62.0%, respectively. In a separate experiment, the crystallization time was extended to 6 h, and the crystallinities for 200 nm nanorods and the bulk were 45.6% and 59.1%, respectively, essentially the same as the results at 2 h. This indicates that the crystallization in the nanorods was complete within 2 h, and the crystallinity difference observed was not due to a unfinished crystallization process in the nanorods. Thus, the crystallinity in the nanorods is significantly lower than that in the bulk for sPS crystallized at higher temperature, and the difference is more dramatic for nanorods of smaller diameter.

Polarized FTIR spectroscopy was then applied to investigate the orientation of the crystalline domains in above cases. The vibrational modes for sPS have been well established.[35,36] For example, a unique feature for sPS is the 1222 cm^{-1} band, which is absent in the spectra of the amorphous and the helical modifications and has been associated with the all-trans planar zigzag backbone conformation. This band is assigned to backbone CCH bending and CC backbone stretching and has a transition dipole moment parallel to the chain axis.[36] Therefore, the 1222 cm^{-1} band can be used to analyze the orientation of the α- and *β*-form crystals. Figure 5 presents the polarized FTIR spectra of different sPS samples in the perpendicular and parallel directions. For the α-form sPS crystallized at lower temperatures (Figure 5A), for both the bulk and the 200 and 80 nm nanorods, the parallel and the perpendicular spectra are almost identical, including the all-trans crystalline band at 1222 cm^{-1}, reflecting the absence of any macroscopic orientation preference for chains in either the amorphous or the crystalline domains. For the *β*-form sPS crystallized at 260 °C, no preferred chain orientation in the amorphous or the crystalline domains in the bulk film is observed either (Figure 5B-a), which is expected. For the 200 and 80 nm nanorod arrays, however, a profound difference is observed in the 1400−800 cm^{-1} region of the spectra of the parallel and perpendicular polarizations (Figure 5B-b,c). The perpendicular bands[36] at 1334, 1028, 1004, and 976 cm^{-1} are much stronger in the parallel polarization than in the perpendicular polarization, while the parallel bands[36] at 1347, 1222, 911, and 858 cm^{-1} are more intense in the perpendicular spectrum. It is interesting to note that the 1222, 911, and 858 cm^{-1} bands are all closely related to the crystalline structure. The band at 1222 cm^{-1} was then used to deduce the orientation of the crystalline domains in the nanorods using eq 1, and the average values of the orientation function F for the 200 and 80 nm nanorods based on four separately prepared film samples were −0.392 and −0.377, showing a high degree of perpendicular orientation. This indicates that the *c*-axis of the *β*-form crystals (which is parallel to the chain axis) preferentially orients perpendicular to the long axis of the nanorods. However, the degrees of orientation are almost the same for the nanorods with different diameters.

To further assess the orientation of the crystals in the nanorods, individual nanorods were isolated and examined by TEM. Figure 6A is the TEM bright field image of a single α-form sPS nanorod and its ED pattern. Only a (211) diffraction circle can be seen in the ED pattern, indicating the presence of α-crystalline domains with no preferred orientation in the nanorod, which accords with the IR results. The TEM bright field image of a single *β*-form sPS nanorod and its ED pattern are shown in Figure 6B. The (020), (040), and (060) diffractions are observed as an array of symmetrical arcs lying along the nanorod direction, which indicates that the (0*k*0) lattice planes

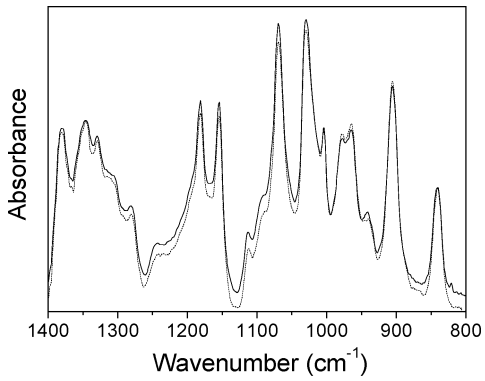

Figure 7. Polarized infrared spectra of sPS nanorods quenched from molten state: perpendicular polarization (—); parallel polarization (---).

are perpendicular to the rod direction, and the *b*-axis of the unit cells aligns along the growth direction of the nanorod. Also observed are a set of (110) and a set of (130) arcs, both very weak, lying close to the rod axis, showing that for some crystals the *b*-axis does not align with the rod direction. However in all cases, the (111) and (041) diffractions, which are strong peaks in the diffraction pattern for the bulk, were not observed. Because the unit cell for the β-form crystals is orthorhombic,[31,32] the diffraction data therefore confirms what we found by polarized IR that the *c*-axis is perpendicular to the axial direction of the nanorod.

It has been proposed that polymer chains adopt a more extended brush configuration where the chain segments orient preferentially perpendicular to the nanopore wall and the tube growth directions when adsorbed from melt to the nanopore walls, which may be responsible for the crystallinity observed.[21] We quenched in ice water an sPS polymer/template assembly in the melt state to freeze the structure and studied by infrared spectroscopy the chain orientation in the nanorods after the template was removed. The sample preparation and measurements were carried out at room temperature, well below the T_g of sPS (~100 °C). Figure 7 displays the polarized IR spectra of the sPS nanorods. The 1222, 851, and 858 cm^{-1} bands characteristic of the crystalline structure are absent, showing that the material in the nanorods is amorphous as expected. No significant difference is observed when comparing the spectra in the parallel and the perpendicular polarizations, which indicates that the polymer chains in the melt state in the nanorods are isotropic with no preferred orientation, and the amount of polymer brushes must be very low if there is any. Therefore, we conclude that the oriented crystallization in the sPS nanorods cannot be attributed to chain orientation in the melt.

It is well-known that at higher crystallization temperatures nucleation is slow, while at lower crystallization temperatures much more nuclei form quickly. When amorphous sPS is heated from room temperature, it starts to crystallize at ~140 °C to form a planar mesomorphic phase, which serves as a template for the growth of the α form.[34] At this temperature the supercooling is very high (~130 °C), and many nuclei form simultaneously with no preferred orientation since the amorphous chains adopt random orientation in the nanorods. These randomly oriented nuclei grow into crystallites while more nuclei form. The randomly oriented crystallites soon bump into each other in the same way as in the bulk, before they grow bigger and feel the confinement of the nanotemplate. Therefore, we observed no significant difference between the nanorods and the bulk in terms of crystallinity and orientation when crystallized at this temperature. On the other hand, for sPS crystallized from the molten state at a high crystallization temperature of 260 °C, i.e., at a very low supercooling (~10 °C), the nucleation is very slow and few nuclei form in a nanopore. Therefore, the stable nuclei formed in the nanopore can grow into big crystals. It is well-known that sPS crystallites grow preferentially in the direction of the *b*-axis, and only the crystals grow along the pore direction can grow bigger while the crystals grow in other directions is suppressed due to the confinement of the pore wall.[22] Therefore, we observed by polarized IR that the chain axis (*c*-axis) orients perpendicular to the rod direction, while [0*k*0], [110], and [130] all can grow along the rod direction with much lower probability, as shown by electron diffraction. The average angle between the crystalline chains and the nanorod direction for the 200 and 80 nm nanorods was 74.7° ($F = -0.392$) and 73.7° ($F = -0.377$), respectively, assuming a uniaxial model, which were almost the same because the preference for the crystal growth direction is the same.

Conclusions

We prepared sPS nanorods of different crystalline forms using anodic aluminum oxide template with various diameters and studied the morphology and the orientation of the polymer in the nanorods using FTIR spectroscopy. In this study FTIR provided a quantitative tool for the analyses of both the chain orientation and the crystallinity. In addition, while X-ray diffraction only examines the crystalline domains, infrared spectroscopy is capable of assessing both the crystalline and amorphous structures, which in this study shows that the polymer chain segments in the melt state in the nanopores prior to crystallization exhibit no preferred orientation. When the amorphous sPS is heated from room temperature and crystallized at lower temperatures, nucleation is the dominating mechanism, and the polymer crystallizes in the nanorods in the same way as that in the bulk, resulting in α-form crystals with the same degree of crystallinity and no preferred orientation. In contrast, for sPS cooled from the molten state and crystallized at low supercooling, while the polymer in the bulk forms β-structure with random orientation, in the nanorods via preferential growth the polymer crystallizes into β-form, with the *c*-axis orienting perpendicular to the axial direction of the nanorod. The crystallinity in the nanorods is significantly lower than in the bulk, and the smaller the pore size, the lower the degree of crystallinity. These findings may be of interest for understanding behavior of polymers under confinement and designing polymeric nanodevices.

Acknowledgment. We thank the National Natural Science Foundation of China (50403008, 20423003) and Jilin Distinguished Young Scholars Program for financial support and Dr. Dorie Yontz of Dow Chemical Co. for supplying the sPS used in this study. Z. Su thanks the NSFC Fund for Creative Research Groups (50621302) for support. Use of the optical microscope in Prof. Men's lab at CIAC is also acknowledged.

References and Notes

(1) Martin, C. R. *Science* **1994**, *266*, 1961.
(2) Martin, C. R. *Chem. Mater.* **1996**, *8*, 1739.
(3) Hulteen, J. C.; Martin, C. R. *J. Mater. Chem.* **1997**, *7*, 1075.
(4) Steinhart, M.; Wendorff, J. H.; Greiner, A.; Wehrspohn, R. B.; Nielsch, K.; Schilling, J.; Choi, J.; Gösele, U. *Science* **2002**, *296*, 1997.
(5) Steinhart, M.; Wehrspohn, R. B.; Gösele, U.; Wendorff, J. H. *Angew. Chem., Int. Ed.* **2004**, *43*, 1334.
(6) Cepak, V. M.; Martin, C. R. *Chem. Mater.* **1999**, *11*, 1363.
(7) Moon, S. I.; McCarthy, T. J. *Macromolecules* **2003**, *36*, 4253.
(8) Ai, S.; Lu, G.; He, Q.; Li, J. *J. Am. Chem. Soc.* **2003**, *125*, 11140.
(9) Liang, Z.; Susha, A. S.; Yu, A.; Caruso, F. *Adv. Mater.* **2003**, *15*, 1849.

(10) Zhang, M.; Dobriyal, P.; Chen, J.; Russell, T. P.; Olmo, J.; Merry, A. *Nano Lett.* **2006**, *6*, 1075.
(11) Shin, K.; Xiang, H.; Moon, S. I.; Kim, T.; McCarthy, T. J.; Russell, T. P. *Science* **2004**, *306*, 76.
(12) Xiang, H.; Shin, K.; Kim, T.; Moon, S. I.; McCarthy, T. J.; Russell, T. P. *Macromolecules* **2004**, *37*, 5660.
(13) Xiang, H.; Shin, K.; Kim, T.; Moon, S. I.; McCarthy, T. J.; Russell, T. P. *J. Polym. Sci., Part B: Polym. Phys.* **2005**, *43*, 3377.
(14) Xiang, H.; Shin, K.; Kim, T.; Moon, S. I.; McCarthy, T. J.; Russell, T. P. *Macromolecules* **2005**, *38*, 1055.
(15) Sun, Y.; Steinhart, M.; Zschech, D.; Adhikari, R.; Michler, G. H.; Gösele, U. *Macromol. Rapid Commun.* **2005**, *26*, 369.
(16) Liang, W.; Martin, C. R. *J. Am. Chem. Soc.* **1990**, *112*, 9666.
(17) Cai, Z.; Lei, J.; Liang, W.; Menon, V.; Martin, C. R. *Chem. Mater.* **1991**, *3*, 960.
(18) Parthasarathy, R. V.; Martin, C. R. *Chem. Mater.* **1994**, *6*, 1627.
(19) Martin, C. R. *Acc. Chem. Res.* **1995**, *28*, 61.
(20) Menon, V. P.; Lei, J.; Martin, C. R. *Chem. Mater.* **1996**, *8*, 2382.
(21) Steinhart, M.; Senz, S.; Wehrspohn, R. B.; Gösele, U.; Wendorff, J. H. *Macromolecules* **2003**, *36*, 3646.
(22) Steinhart, M.; Göring, P.; Dernaika, H.; Prabhukaran, M.; Gösele, U.; Hempel, E.; Thern-Albrecht, T. *Phys. Rev. Lett.* **2006**, *97*, 027801.
(23) Hu, Z.; Baralia, G.; Bayot, V.; Gohy, J.-F.; Jonas, A. M. *Nano Lett.* **2005**, *5*, 1738.
(24) Huang, P.; Zhu, L.; Cheng, S. Z. D.; Ge, Q.; Quirk, R. P.; Thomas, E. L.; Lotz, B.; Hsiao, B. S.; Liu, L. Z.; Yeh, F. J. *Macromolecules* **2001**, *34*, 6649.
(25) Huang, P.; Guo, Y.; Quirk, R. P.; Ruan, J.; Lotz, B.; Thomas, E. L.; Hsiao, B. S.; Avila-Orta, C. A.; Sics, I.; Cheng, S. Z. D. *Polymer* **2006**, *47*, 5457.
(26) Ishihara, N.; Seimiya, T.; Kuramoto, M.; Uoi, M. *Macromolecules* **1986**, *19*, 2464.
(27) Zambelli, A.; Longo, P.; Pellecchia, C.; Grassi, A. *Macromolecules* **1987**, *20*, 2035.
(28) Su, Z.; Li, X.; Hsu, S. L. *Macromolecules* **1994**, *27*, 287.
(29) Kobayashi, M.; Nakaoki, T.; Ishiraha, N. *Macromolecules* **1989**, *22*, 4377.
(30) Guerra, G.; Vitagliano, V. M.; De Rosa, C.; Petraccone, V.; Corradini, P. *Macromolecules* **1990**, *23*, 1539.
(31) De Rosa, C.; Rapacciuolo, M.; Guerra, G.; Petraccone, V.; Corradini, P. *Polymer* **1992**, *33*, 1423.
(32) Chatani, Y.; Shimane, Y.; Ijitsu, T.; Yukinari, T. *Polymer* **1993**, *34*, 1625.
(33) Greis, O.; Xu, Y.; Asano, T.; Petermann, J. *Polymer* **1989**, *30*, 590.
(34) Handa, Y. P.; Zhang, Z.; Wong, B. *Macromolecules* **1997**, *30*, 8499.
(35) Kellar, E. J. C.; Galiotis, C.; Andrews, E. H. *Macromolecules* **1996**, *29*, 3515.
(36) Reynolds, N. M.; Hsu, S. L. *Macromolecules* **1990**, *23*, 3463.
(37) Masuda, H.; Fukuda, K. *Science* **1995**, *268*, 1466.
(38) Sauer, G.; Brehm, G.; Schneider, S.; Nielsch, K.; Wehrspohn, R. B.; Choi, J.; Hofmeister, H.; Gösele, U. *J. Appl. Phys.* **2002**, *91*, 3243.
(39) Sun, Y. S.; Woo, E. M. *Macromolecules* **1999**, *32*, 7836.
(40) Koenig, J. L. *Spectroscopy of Polymers*, 2nd ed.; Elsevier: New York, 1999.
(41) Wu, H. D.; Wu, I. D.; Chang, F. C. *Macromolecules* **2000**, *33*, 8915.
(42) Wu, H. D.; Wu, S. C.; Wu, I. D.; Chang, F. C. *Polymer* **2001**, *42*, 4719.
(43) Wu, H. D.; Tseng, C. R.; Chang, F. C. *Macromolecules* **2001**, *34*, 2992.

MA070564O